

Tailoring the work function of graphene via defects, nitrogen-doping and hydrogenation: A first principles study

Nikolay Dimov¹ , Aleksandar Staykov^{1,2} ,
Muhammad Irfan Maulana Kusdhany³  and Stephen M Lyth^{1,3,4,5,6,7,*} 

¹ International Institute for Carbon-Neutral Energy Research (WPI-I2CNER), Kyushu University, 744 Motoooka, Nishi-ku, 819-0395, Fukuoka, Japan

² Department of Chemical Engineering, Kyushu University, 744 Motoooka, Nishi-ku, 819-0395, Fukuoka, Japan

³ Department of Automotive Science, Kyushu University, 744 Motoooka, Nishi-ku, 819-0395, Fukuoka, Japan

⁴ Next-Generation Fuel Cell Research Center, Kyushu University, 744 Motoooka, Nishi-ku, 819-0395, Fukuoka, Japan

⁵ Department of Chemical and Process Engineering, University of Strathclyde, Glasgow G1 1XL, United Kingdom

⁶ Department of Mechanical and Mining Engineering, University of Queensland, St Lucia QLD 4072, Australia

⁷ Department of Mechanical Engineering, University of Sheffield, Sheffield S1 3JD, United Kingdom

E-mail: lyth@kyudai.jp and alex@i2cner.kyushu-u.ac.jp

Received 29 March 2022, revised 31 May 2022

Accepted for publication 6 July 2022

Published 25 July 2023



CrossMark

Abstract

The effect of defects, nitrogen doping, and hydrogen saturation on the work function of graphene is investigated via first principle calculations. Whilst Stone–Wales defects have little effect, single and double vacancy defects increase the work function by decreasing charge density in the π -electron system. Substitutional nitrogen doping in defect-free graphene significantly decreases the work function, because the nitrogen atoms donate electrons to the π -electron system. In the presence of defects, these competing effects mean that higher nitrogen content is required to achieve similar reduction in work function as for crystalline graphene. Doping with pyridinic nitrogen atoms at vacancies slightly increases the work function, since pyridinic nitrogen does not contribute electrons to the π -electron system. Meanwhile, hydrogen saturation of the pyridinic nitrogen atoms significantly reduces the work function, due to a shift from pyridinic to graphitic-type behavior. These findings clearly explain some of the experimental work functions obtained for carbon and nitrogen-doped carbon materials in the literature, and has implications in applications such as photocatalysis, photovoltaics, electrochemistry, and electron field emission.

Supplementary material for this article is available [online](#)

Keywords: work function, carbon, defect chemistry, nitrogen-doped carbon, nitrogen-doped graphene, electrochemistry, hydrogenated graphene

(Some figures may appear in colour only in the online journal)

* Author to whom any correspondence should be addressed.



Original content from this work may be used under the terms of the [Creative Commons Attribution 4.0 licence](#). Any further distribution of this work must maintain attribution to the author(s) and the title of the work, journal citation and DOI.

Introduction

Graphene is a graphitic carbon material with interesting properties arising from its unique structure, leading to a wide variety of applications. It is defined as a freestanding infinite monolayer of graphite with a hexagonal crystal lattice.

However, experimentally produced graphene is generally far from perfect, and the measured properties often deviate significantly from the predicted behavior. For example, adsorbed gas or solvent molecules, and the influence of the support have a strong impact on the measured properties. In particular, defects in the crystal lattice are almost unavoidable. These have an impact on e.g. the mechanical strength due to disruption of the covalent binding network [1], or the electronic properties due to disruption of the sp^2 π -electron network. Defects thus have an impact on applications like photocatalysis, electrocatalysis, electronics, and photovoltaics. As such, the effect of defects on the properties of graphene should be clarified.

In principle, there are an unlimited number of structural combinations that can be formed in the graphene lattice, and a very large number of possible defect structures [2]. However, common defect structures can be narrowed down to: (1) Stone–Wales; (2) single vacancies; (3) double vacancies; and (4) carbon adatom defects [3]. The Stone–Wales defect does not involve adding or removing of carbon atoms, but originates from the rearrangement of four adjacent hexagons into two pentagons and two heptagons by the rotation of a C–C bond by 90° . Single vacancy defects (or mono-vacancies) are formed by removing a single atom from the carbon lattice [4]. This would leave three carbon atoms with dangling bonds, but two of these are saturated due to Jahn–Teller distortion [5]. The remaining bond cannot be saturated due to geometric effects but is generally terminated by e.g. hydrogen ions in the local environment. Double vacancies (or divacancies) are formed by removal of two carbon atoms from the lattice and rearranging the bond lengths to minimize strain. Double vacancy defects are generally almost flat, since they mainly accommodate bond strain by adjusting both bond length and bond angle. Since there are no dangling bonds, double vacancies are relatively stable. Removing more than two atoms can yield more complex and larger defect configurations. As a rule of thumb, removing an even number of atoms from pristine graphene will result in fully saturated defects, whilst an odd number of missing atoms results in unsaturated bonds. Interstitial adatoms cannot exist in graphene, because placing an extra atom in the plane of the graphene sheet would require prohibitively high energy. Therefore, carbon adatom defects in graphene are located out-of-plane. The simplest carbon adatom defects are the bridge and dumbbell configurations. The bridge configuration has a dangling bond and can therefore form covalent bonds, whilst the dumbbell configuration is saturated and stable. In the real world, graphitic carbon materials will contain a certain distribution of vacancies and defects. Larger defect structures can be approximated with combinations of the aforementioned defects, which are sufficient to represent the properties of various structural motifs.

One of the key properties of defective graphenic materials is their work function. This is defined as minimum energy needed to remove an electron from a material to a point immediately outside the surface, and is equivalent to the difference between the vacuum energy (E_{vac}) and the Fermi

level (E_F) [6]. The work function is a fundamental property of graphene and has important implications for the performance in applications such as field effect tunneling transistors, optical modulators, transparent electrodes for touch panels, and organic solar cells. Experimental determination of the work function can be obtained by various methods. Absolute methods include ultraviolet photoelectron spectroscopy (UPS), thermionic emission and field emission, whilst Kelvin probe microscopy is a relative method [7–10]. However, many different experimental values have been reported for graphene, ranging from 3.7 to 5.2 eV [11], highlighting the issues faced when measuring work function. The precise chemical structure of the specific graphene material being studied should be considered. Defects, edges, and dopants are expected to impact the result. The effect of the substrate and/or adsorbents should be also taken into consideration. Recently, the work function of suspended CVD-grown polycrystalline graphene measured using thermionic emission to avoid both substrate effects and adsorbent effects was measured to be 4.74 eV, in one of the most reliable estimates to date [11]. *However, more theoretical insight into the absolute work function of different graphene defect structures and dopants is needed.*

Various techniques have been used to tune or engineer the work function of graphene. For example, the work function of mechanically exfoliated graphene on SiO_2 substrates was varied between 4.78 and 4.47 eV by taking advantage of the electric field effect [9]. α -beam (He^{2+}) irradiation has been used to create atomic scale defects in monolayer CVD-grown graphene on copper substrates, resulting in an increase in work function from 4.5 eV to 4.9 eV [12]. The work function of graphene oxide (GO) on indium tin oxide (ITO) substrates was varied from 5.4 eV to 4.5 eV (measured by UPS) by heating in vacuum to produce reduced graphene oxide (rGO), highlighting the importance of functional groups on the electronic structure [13]. CVD-grown few-layer graphene on nickel substrates was coated with Au nanoparticles to increase the work function by 0.5 eV [14]. The work function of CVD-grown graphene was lowered to 3.9 eV after transfer onto an SiO_2 substrate modified with a layer of self-assembled molecules (SAMs), compared with 4.5 eV for graphene directly on SiO_2 [15]. The work function of few-layer graphene sheets doped with Li_2CO_3 , K_2CO_3 , Rb_2CO_3 , or Cs_2CO_3 decreased from 4.3 to 3.8, 3.7, 3.5, and 3.4 eV, respectively [16]. A uniaxial strain of 7% in CVD-grown graphene was used to increase the work function by 0.16 eV [17]. Work function variations of 30 meV have also been observed at line defects in CVD-grown graphene transferred onto SiO_2 substrates at grain boundaries, standing collapsed wrinkles, and folded wrinkles [18]. *The mechanisms behind these changes in work function should be investigated in more detail.*

Another key method of changing the work function of graphene and other carbons is by doping with heteroatoms. For example, the measured work function of CVD-grown graphene has been decreased from 4.91 to 4.37 eV via nitrogen plasma treatment, attributed to graphitic nitrogen incorporated in the graphene sheet [19]. Similarly, nitrogen

plasma treatment of highly crystalline pristine graphene and defective graphite surfaces resulted in nitrogen doping at either graphitic or pyridinic sites, respectively. In this case, an initial decrease in work function was observed in the pristine sample for substitutional nitrogen doping, but for longer plasma treatment times the work function increased in both cases, attributed to the formation of defects [20]. *The effect of nitrogen-doping should be investigated at a fundamental level to gain insight into the mechanisms behind these changes.*

In this work, we consider various defect and nitrogen-doped defect configurations in a simulated graphene layer approximated with an array of 70–72 atoms. This size is sufficient to accommodate most simple defects described in the literature [2]. First, we systematically introduce the most common defects in graphene. We then create models of these defects, evaluate their formation energies (i.e. their relative stability), and explore the changes they induce on the work function of graphene. Then we consider substitutional doping of graphitic nitrogen and doping of pyridinic nitrogen atoms at defects, and discuss the interplay between nitrogen-doping, the stability of nitrogen-doped defects, the nitrogen content, and the work function. We also consider defects with dangling bonds, and the effect of hydrogen saturation on the defect stability and work function.

Computational methods

Density functional theory (DFT) calculations were performed using the Perdew–Burke–Ernzerhof (PBE) exchange–correlation functional. The first step of the simulation was to fully relax the ground-state geometries of all defect- and nitrogen-doped defect containing structures. All defective graphene sheets were calculated as 3D-periodic models, which are 2D sheets on x – y plane with a 15 Å vacuum slab along the z -axis to decouple the images. The projector-augmented wave (PAW) method, as implemented in the Vienna *Ab-initio* Simulation Package (VASP), was used to evaluate the electron-ion interactions with a plane-wave cutoff energy of 400 eV [21–24]. The k -points were generated using a $3 \times 3 \times 1$ Monkhorst-Pack algorithm. Spin polarization was included in the calculations. A well-documented drawback of the PBE exchange–correlation functional is underestimation of computed band gaps in materials containing transition metals. However, transition metals are not included in this study, and large deviation related to the type of the exchange–correlation functional used in the computations are not expected. Future work including the use of various exchange–correlation potentials, such as PBE0, HSE, or Meta-hybrid GGA, as well as inclusion of transition metals would be a logical continuation of this work.

Defect formation energies were calculated from the following equation:

$$\Delta E_o(d) = E_d - E_o + n_C \mu_C - n_H \mu_H - n_N \mu_N, \quad (1)$$

where $\Delta E_o(d)$ is the energy required to form the defect; E_d is the total energy of the defect-containing supercell; and E_o is the total energy of pristine graphene supercell (i.e. -664.7427 eV

for C_{72}). μ_C , μ_H and μ_N are the chemical potentials of C, H, and N, respectively, calculated from first principles to be: $\mu_C = -9.267$ eV, $\mu_H = -3.350$ eV, and $\mu_N = -8.30$ eV n is the number of doped atoms.

Convergence criteria for the energy and force were set to 0.001 eV and 0.01 eV Å⁻¹, respectively. The graphical visualization package VESTA was used to analyze and visualize the computational results [25]. The vacuum energy surrounding the graphene sheets was determined by a line profile tool available in VESTA. A qualitative criterion for decoupled 3D images is the presence of a flat region in the line profile between images. The work function was then calculated as the difference between the vacuum and Fermi levels:

$$\Phi = E_{\text{vac}} - \varepsilon_f, \quad (2)$$

where Φ denotes the work function, E_{vac} is the energy of the vacuum as calculated by the DFT implementation in VASP, and ε_f is the Fermi energy. This agrees with the physical definition of the work function given above.

Results and discussion

Structure and distribution of bond lengths

Figure 1 summarizes the different graphene defect structures investigated in this study, after relaxation. The defect naming convention is based on the number and type of non-hexagonal rings, after Banhart *et al* [2]. The ideal graphene lattice is shown in (a). The 55-77 Stone–Wales defect in (b) is a fully saturated point defect. The 5-9 defect in (c) is a single vacancy defect with unsaturated bonds. The 585 defect in (d), the 555-777 defect in (e), and the 5555-6-7777 defect in (f) are all fully-saturated double vacancies. The dumbbell and bridge adatom defects in (g) and (h), respectively, are both unsaturated. *The defects studied here, or combinations thereof, can approximate most of the structures present in physical systems.*

The presence of the above defects in the graphene structure generates a variety of C–C bonds in the crystal lattice with slightly different lengths (figure S1 (available online at stacks.iop.org/NANO/34/415001/mmedia)). In the case of pristine graphene (a), all the bond lengths are 1.42 Å in agreement with the literature [3]. The Stone–Wales defect (b) has a range of bond lengths distributed around the same value. For the 5-9 defect (c), most bond lengths are 1.45 Å, but 2 bonds are much shorter (~ 1.35 Å) and one bond is much longer (~ 2.50 Å). The distribution of bond lengths in the other defect structures can be seen in the graphs. *This variation in bond length is important, as it results in a redistribution of charge in the π -electron system.* This in turn will have an impact on the work function, since the charge is intimately linked with the definition of Fermi level.

Defect formation energies

The formation energies of different defect structures relate to the probability that they will be found in nature. If the

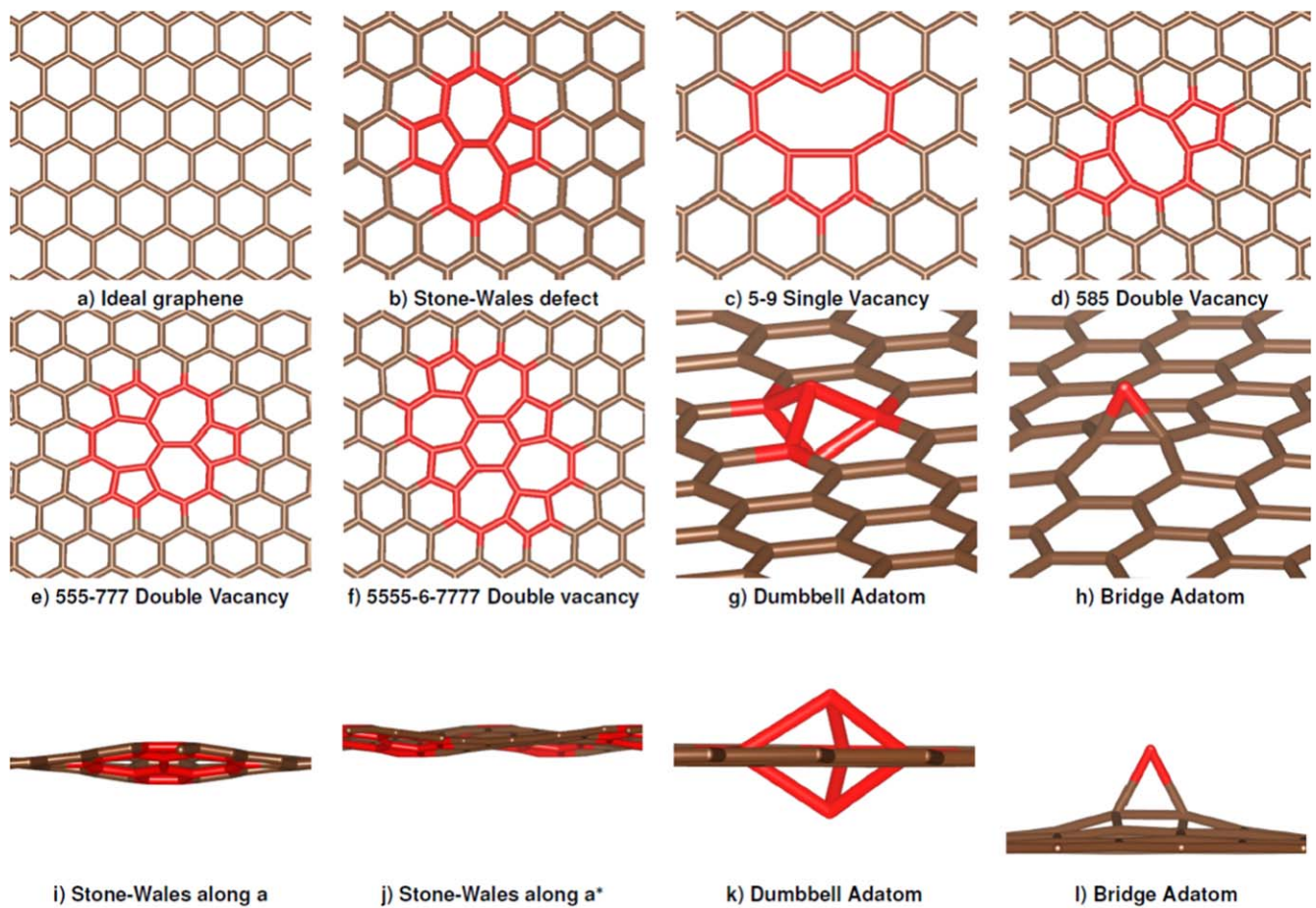


Figure 1. Overview of the graphene defect structures simulated here. (i)–(j): Side views of the non-planar optimized Stone–Wales defect along the a and a^* axes. (k)–(l): Side views of the non-planar optimized dumbbell and bridge adatom defects. Carbon atoms contributing to the defect structure are depicted in red, whilst those not directly contributing are depicted in brown. For clarity, hydrogen saturation of the 5-9 and bridge adatom defects is not shown.

Table 1. Total energy of formation of the superlattice, E_d ; the defect formation energy, $\Delta E_0(d)$; and the work function of the defective graphene structures depicted in figure 1. Black, blue, red, and green correspond to Stone–Wales, single vacancy, double vacancy, and adatom defects, respectively.

Superlattice	E_d/eV	$\Delta E_0(d)/eV$	Work function/eV
Defect-free graphene	−664.74	0	4.30
Stone–Wales (55-77)	−659.79	4.95	4.30
Single vacancy (5-9)	−647.88	7.63	4.49
1H single vacancy (5-9)	−652.13	5.65	4.36
3H single-vacancy (5-9)	−662.57	−0.28	4.19
Double vacancy (585)	−638.52	7.76	4.40
Double vacancy (555-777)	−639.79	6.49	4.72
Double vacancy (5555-6-7777)	−638.79	7.49	4.50
Dumbbell adatom	−667.13	6.84	4.39
Bridge adatom	−667.51	6.47	4.54
2H bridge adatom	−678.72	−0.23	4.15

formation energy is too high, it is unlikely that the defect will form, and vice versa. This can be broadly translated to the relative abundance of different types of defects in real-world graphitic carbon samples. Table 1 lists the calculated formation energies of the different defects studied here. For pristine graphene, there is no formation energy since this is the reference point. The 55-77 Stone–Wales defect is formed without the addition or removal of any carbon atoms, and the formation energy is 4.95 eV. The 5-9 single vacancy defect is chemically unstable with a formation energy of 7.63 eV, due to the unsaturated dangling bond. The formation energies of the same 5-9 vacancy terminated with 1 or 3 hydrogen atoms are 5.65 and −0.28 eV, respectively. The negative value of the 3H 5-9 defect reflects that the formation of this hydrogen-terminated structure is highly favorable. Of the three fully saturated double vacancies, formation of the 555-777 defect is most energetically favorable. Formation of the dumbbell and unsaturated adatom defects are both relatively unfavorable at 6.84 and 6.47 eV, respectively. Again, hydrogen-termination of the bridge adatom defect results in a much more favorable structure, with a formation energy of −0.23 eV. Overall, the formation energy of the Stone–Wales defect is several

electron volts lower than for the cases of single or double vacancies. This is consistent with previous studies, and validates the computational techniques used in this study [2].

Work function of defective graphene

The work functions were calculated as the difference between the vacuum energy and the Fermi level (table 1). Pristine graphene is calculated to have a work function of 4.30 eV. The Stone–Wales defect has the same work function, because it is simply a rearrangement of bonds, and the π -electron system is not perturbed. Meanwhile, almost all of the defect structures have work functions higher than pristine graphene. This is because vacancies do not donate electrons to the π -electron system, resulting in an electron deficiency that increases the amount energy required to remove a single electron from the surface to infinity. The biggest increase in work function is observed for the 555-777 double vacancy defect (4.72 eV).

The experimentally measured work function of graphene ranges from 3.7 to 5.2 eV, and one of the most reliable recent studies measured a value of 4.74 eV [11.] Our value for pristine graphene is within this range, but is lower than most of the reported studies. *Our results suggest that the unavoidable presence of defects in graphene results in artificially high measurements of the work function in the lab.* Indeed, increase of the work function due to defects has been already observed experimentally, where α -beam irradiation increased the work function from 4.5 eV to 4.9 eV [26].

Interestingly, two of the hydrogen-terminated defect structures have slightly lower work function compared to pristine graphene (i.e. the 5-9 3H single vacancy, and the 2H bridge adatom defect). This is because hydrogen atoms donate electrons to the structure, shifting the Fermi level by up to 0.25 eV. Similar results have been reported in the experimental literature, where the work function of hydrogenated carbon is decreased [27, 28].

Substitutional nitrogen doping

Herein, we investigate the effect of nitrogen doping on the work function of graphene. First, we consider substitutional doping of nitrogen atoms into pristine graphene by simply replacing carbon atoms with nitrogen atoms. The interaction energy between adjacent substitutional nitrogen atoms was first calculated as a function of the N–N distance within the lattice, to estimate which configurations are most energetically favorable (figure S2(a)). In all cases of substitutionally doped nitrogen, the work function is much lower than that of pristine graphene, regardless of the configuration. There is only a weak trend of increasing work function with N–N proximity (figure S2(b)). The reduction in work function is due substitutional nitrogen atoms contributing two electrons to the π -electron system from their p_z orbital. This increases the π -electron density, shifting the Fermi level and making it easier to remove an electron. This result is in agreement with the experimental literature, where e.g. nitrogen plasma treatment was reported to reduce the work function of CVD-

grown graphene by 0.5 eV [19], which is similar to the change of ~ 0.7 eV observed here.

Positions 1–5 (i.e. an N–N distance of 4.3 Å) were selected as representative for calculating the work function with increasing nitrogen content, as a trade-off between the supercell size and the N–N interaction energy (figure 2). The work functions of nine different structures were calculated, increasing the nitrogen content in the supercell whilst maintaining a constant N–N separation. The results clearly show that the work function is highly sensitive to the nitrogen content (figure 3). The first nitrogen atom doped into the C_{72} graphene supercell (corresponding to 1.4 at%) results in a large decrease in work function from 4.30 to 3.64 eV. Addition of further nitrogen atoms leads to a more gradual decrease in work function. In the case of 8 nitrogen atoms per supercell (11.1 at%), the work function is 3.25 eV, which is a decrease of 1.05 eV compared to pristine graphene. Increasing the concentration any more would result in an uneven distribution of nitrogen atoms, leading to clustering.

This trend in work function can be explained as follows. The first nitrogen atom doped into the graphene sheet donates an electron from the p_z orbital to the π -electron system, causing an upshift in the Fermi level, as observed in the DOS (figure S3). Each additional nitrogen atom donates another electron to the π -electron system, with a corresponding reduction in work function. However, the Fermi level changes by a smaller increment with each electron added, because of the increased integrated DOS area of the π^* levels of graphene as the energy increases above the Fermi level.

Graphitic/tertiary nitrogen doping at defects

Next, the effect of nitrogen doping at defects in graphene was considered. There are many possible types of defects. Doping all of these with nitrogen would result in an unmanageable range of possible structures. Therefore, we selected the 585 double vacancy as representative, and the calculated chemical structures are shown in figures S4–S6. Other defect structures were probed in less detail, and the same general trends were observed (not shown).

Figure 3 plots the change in work function with increasing nitrogen content for graphitic (blue triangles) nitrogen atom substitution. It is immediately clear that the trend is different from the case of substitutional nitrogen doping (black squares). The work function of the undoped 585 defect (i.e. 4.4. eV) is slightly higher than that of the pristine graphene sheet, as discussed earlier. This is because the π -electron system is deficient by 2 electrons due to the double vacancy, increasing the work needed to remove an electron from the surface.

Doping the 585 double vacancy with 1 substitutional nitrogen atom per supercell (1.4 at%) donates an electron to the π -electron system, but the system is still electron deficient compared to pristine graphene, because of the double vacancy. As such the work function does not significantly change. Doping with 2 nitrogen atoms per supercell (2.8 at% nitrogen) results in a slight decrease in work function. In this case, two electrons are donated to the supercell π -electron

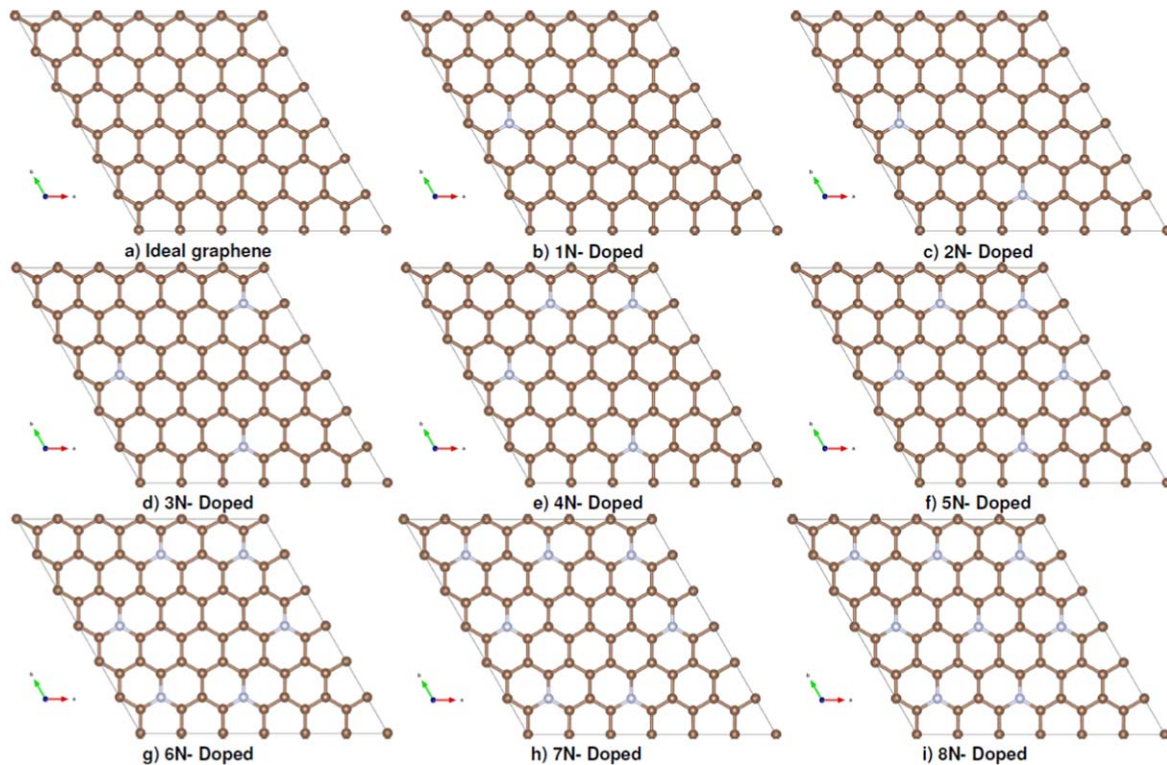


Figure 2. Schematic of nine different structures used to investigate the effect of nitrogen content on the work function. The supercell size was 72 atoms, and the N–N distance was fixed at ≥ 4.3 Å to minimize N–N repulsion.

system, replacing those unaccounted for by the 585 double vacancy. As such, the work function is similar to that of pristine graphene. When 3 atoms are added per supercell (4.2 at%) the work function falls to 3.8 eV, because of the excess electron added to the π -electron system. As the number of atoms per supercell increases further, there is only a gradual decrease in the average work function, despite progressively injecting more electrons into the π -electron system. This is due to saturation and degeneration of the π -electron system.

Pyridinic nitrogen doping at defects

Figure 3 also plots the change in work function with increasing nitrogen content, for pyridinic substitution (red diamonds). The situation for pyridinic doping at the edges of the 585 double vacancy is dramatically different. In this case, the average work function actually increases steadily as the number of nitrogen atoms per supercell increases. This can be explained by the electronic structure of pyridinic nitrogen atoms. Contrary to the case of substitutional graphitic nitrogen where the p_z -orbital is occupied with two electrons, the lone pair of pyridinic nitrogen populates the sp^2 -orbitals, which are oriented in the plane of the graphene sheet. As such, they do not overlap with the π -electron system and cannot populate it with extra electrons, and the work function does not decrease.

This data shows that work function engineering is highly sensitive to the presence of defects, as well as the type of nitrogen doping, i.e. graphitic or pyridinic. Compared with substitutional nitrogen doping in defect-free graphene, the

work function of defective graphene is higher over the whole range. The total achievable change in work function for pristine graphene was ~ 1.0 eV, compared with only ~ 0.6 eV if defects are present, and potentially much less if a mix of pyridinic and graphitic nitrogen are present, as is expected in real-world samples. Much more nitrogen doping in defective graphene is required to achieve similar change in work function as the pristine case. *As such, more crystalline forms of carbon with a high proportion substitutionally doped nitrogen should be used for applications requiring low work function.* In practice, this could mean selecting crystalline nitrogen-doped carbons grown by e.g. chemical vapor deposition (CVD), rather than doping carbon via e.g. heating in ammonia, or nitrogen plasma irradiation. Similar results are seen in the literature, with substitutional nitrogen-doped carbon having a work function of 4.3 eV, compared to 5.4 eV for defective nitrogen doped carbon [20]. This conclusion has implications for applications where the work function is important, e.g. organic light emitting diodes (OLEDs), organic photovoltaics, photocatalysis, electron field emission, and electrochemistry.

Clustered nitrogen defects

The clustering of nitrogen atoms in carbon has frequently been reported to be energetically favorable in the computational literature, but imaging such clusters experimentally remains challenging. For example, Hou *et al* reported that pyridinic nitrogen-substitution is energetically favorable at defects, and that trimerized 3N-pyridine defects have

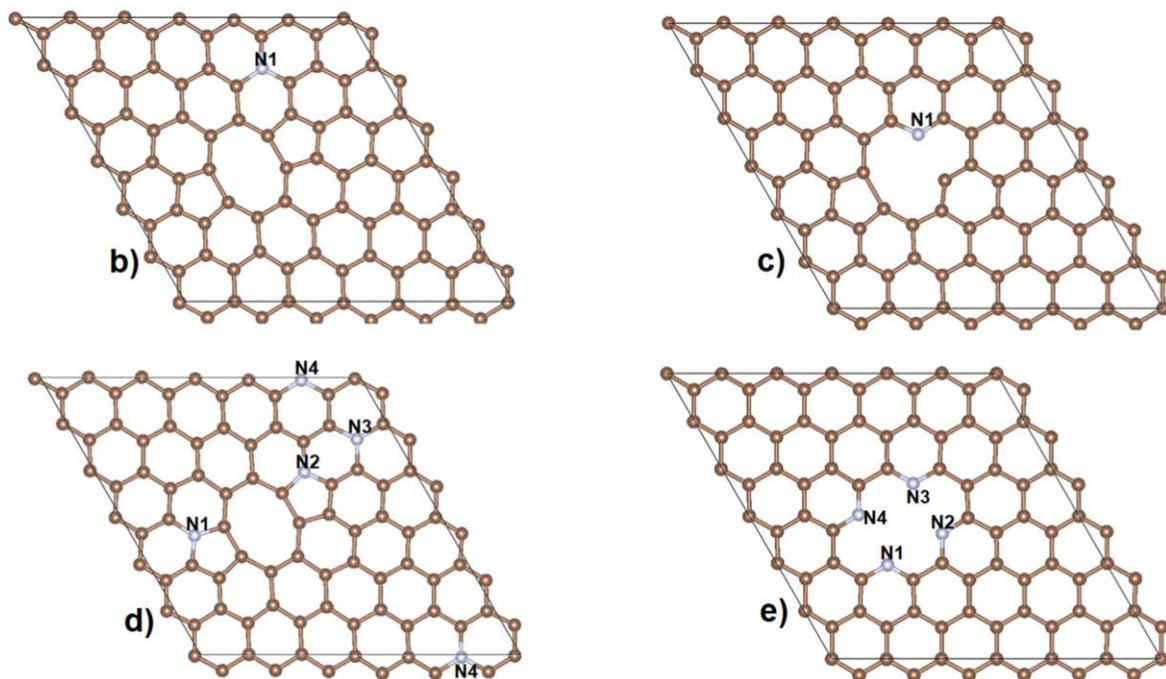
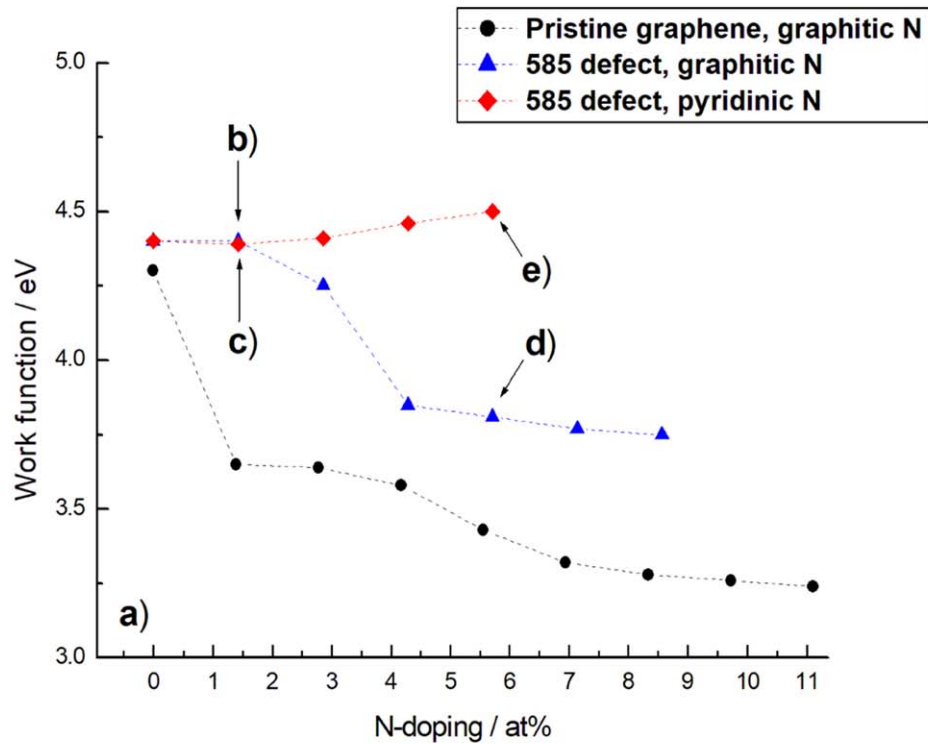


Figure 3. (a) Graph showing the change in work function with nitrogen content for: substitutional nitrogen doping (black circles); graphitic nitrogen doping of a 585 defect (blue triangles); and pyridinic nitrogen doping at the edges of a 585 defect. Values are averaged for multiple structures with the same number of nitrogen atoms in the unit cell (see SI), (b) and (d) 1N- and 4N-substitutional nitrogen doping, (c) and (e) 1N- and 4N-pyridinic nitrogen doping. Note that (b) and (d) are just some of the many possible structures, while (c) and (e) are the only possibilities.

particularly high stability [29]. Similarly, Fujimoto *et al* studied nitrogen defects in carbon nanotubes and graphene, finding that pyridinic nitrogen is more easily incorporated near defects, and that the formation energy of trimerized 3N-pyridinic nitrogen is lower than all other possible pyridinic

formations [30]. 1N- and 2N-pyridinic defects have been observed experimentally using scanning tunneling microscopy [31]. Meanwhile, 4N-pyridinic ‘defects’ are commonly found in nature in the form of heterocyclic macrocycle organic compounds such as porphyrins (for example heme, or

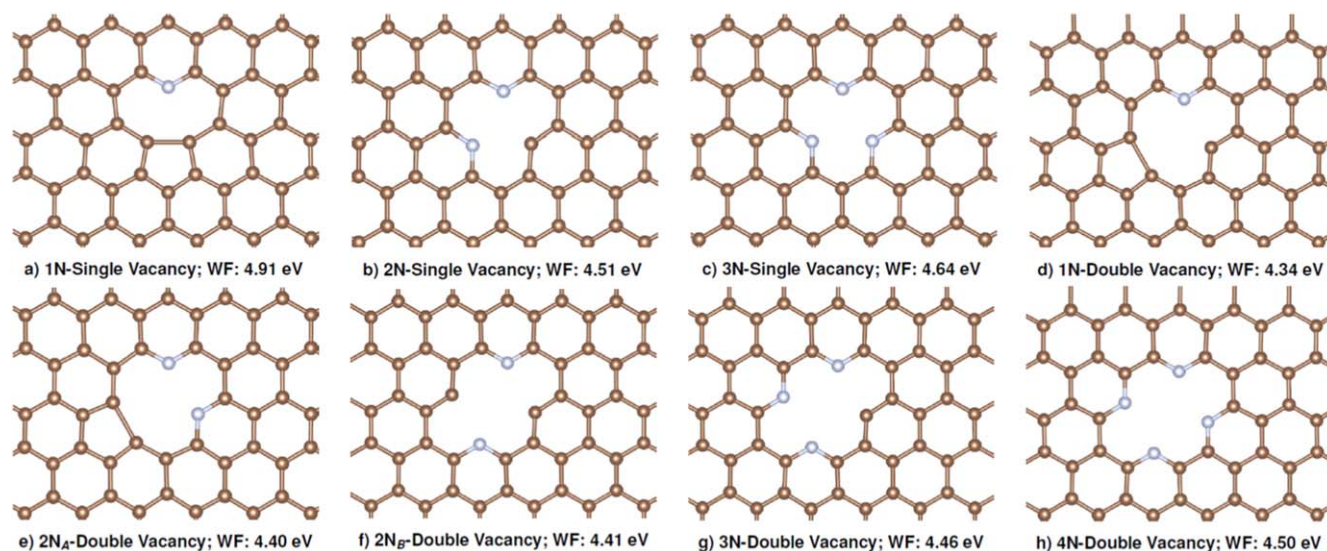


Figure 4. Summary of the clustered pyridinic nitrogen-doped graphene defect structures: (a) 1N-; (b) 2N-; and (c) 3N-single vacancy defects; (d) 1N-, (e) 2N_A-, (f) 2N_B-, (g) 3N- and (h) 4N-double vacancy defects. There is no significant shift in the Fermi level or reduction in the work function for any of these structures (see table S5).

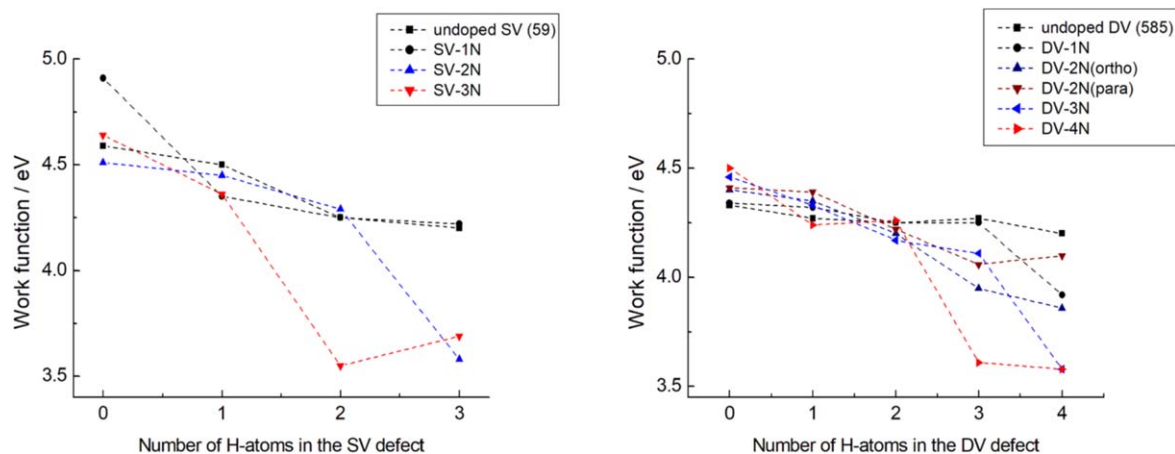


Figure 5. Variation in the work function for nitrogen-doped vacancies in graphene, with sequentially increasing hydrogen saturation: (a) single vacancies; and (b) 585 double vacancies. All of the calculated structures are shown in the supporting information.

phthalocyanines). Such structures are widely used as biocatalysts in nature, or in artificial systems, e.g. photocatalysis. Similarly, the active site of Fe–N–C platinum-free electrocatalysts for the oxygen reduction reaction are believed to comprise FeN_{2/4} clusters (i.e. 2N- or 4N-pyridinic clusters coordinated to an Fe atom) [32, 33].

The structures of pyridinic 1N-, 2N-, 3N-, and 4N single and double vacancies in the graphene supercell are shown in figure 4. The formation energies of these structures relative to pristine graphene are shown in table S5. The formation energies reflect the relative stability of the different structures, with the 3N single vacancy and the 4N double vacancy structures being the most stable. The undoped double (585) and single (59) vacancies are the least stable. Therefore, it is evident that clustering of pyridinic N-atoms in double and single vacancy defects is energetically favorable, and tends to stabilize the structures, in agreement with previous studies [29]. Meanwhile, the work function slightly increases when the single and double vacancy

structures are doped with pyridinic nitrogen atoms, because they do not contribute electrons to the π -electron system, as previously discussed (figure S7). *As such, clustering of unsaturated pyridinic nitrogen at defects is not an effective way to engineer the work function.*

Hydrogen saturation of clustered nitrogen defects

First principle studies by Hou *et al* previously suggested that hydrogen saturation stabilizes the single vacancy defect [29]. Here, we extend this study to the double vacancy, explore the effect of hydrogen saturation of pyridinic nitrogen doped at defects and determine the influence of hydrogen saturation on the work function. A full list of the doped and hydrogenated single and double vacancy defects studied is summarized in figures S8–S17, and tables S6–S15. As expected, the general trend is that hydrogenation increases the stability. The trend in work function for single and double vacancies with increasing hydrogen saturation is summarized in figure 5. As discussed

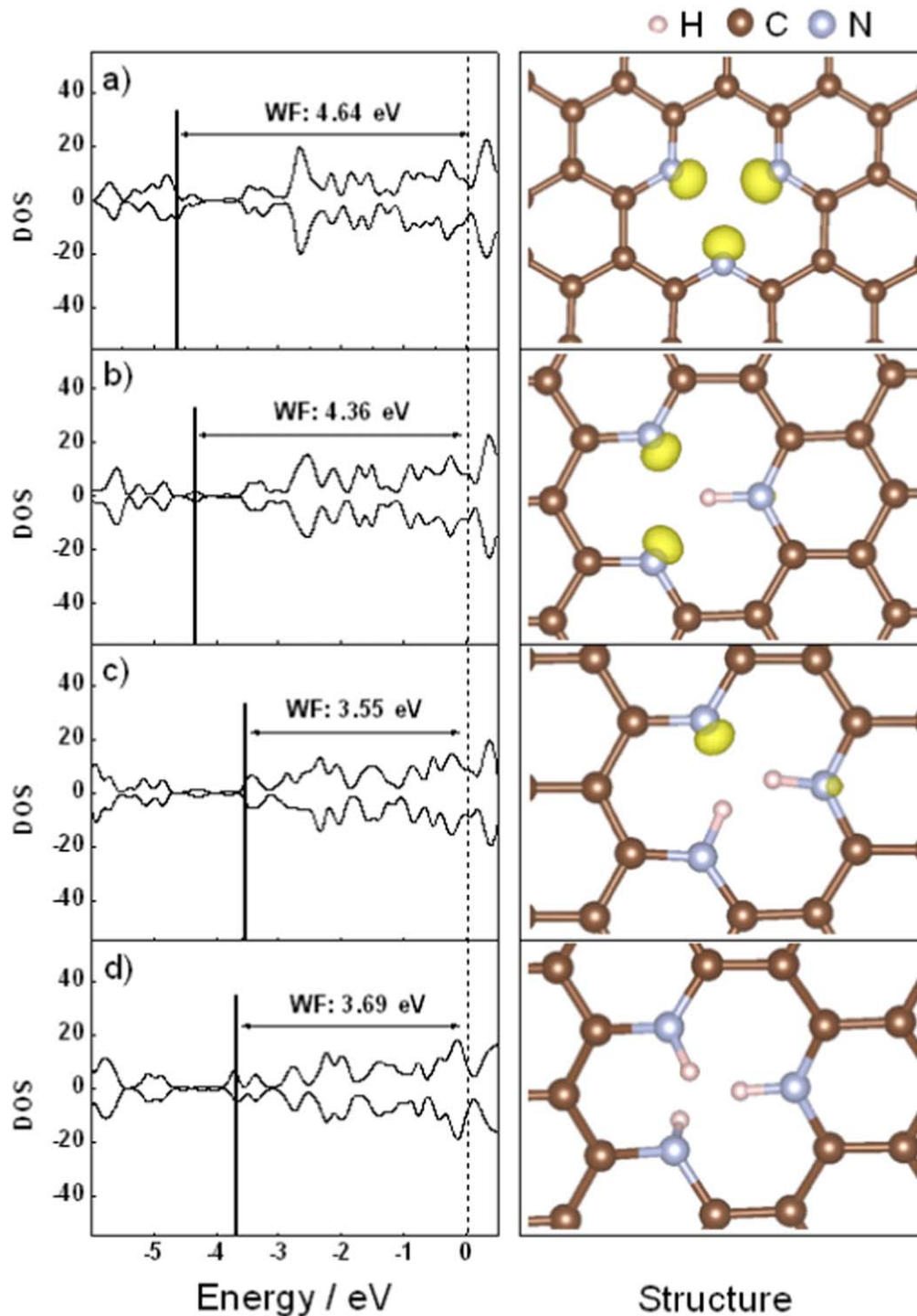


Figure 6. Density of states and work function for a sequentially hydrogenated single vacancy 3N-defect: (a) 0H⁻; (b) 1H⁻; (c) 2H⁻; and (d) fully hydrogenated 3H⁻.

above, pyridinic nitrogen does not significantly affect the work function of graphene. However, hydrogen saturation of clustered nitrogen defects does lead to a clear reduction in work function. When saturating pyridinic nitrogen, the single p_y electron of the pyridinic nitrogen forms a bond with the hydrogen atom. This shifts the system from pyridinic-type behavior to graphitic type behavior, because the resulting electron pair interacts with the π -electron system (figure 6). The end result is similar to the case when graphitic nitrogen

atoms are incorporated into the graphene. As such, hydrogenation of nitrogen-doped carbons may be an effective method for engineering the work function.

Summary and conclusions

The dependence of the work function of graphene on defects, nitrogen doping, and hydrogen saturation was investigated

from first principles. The work function of pristine graphene was 4.3 eV. Stone–Wales defects had the same work function, since the π -electron system is unperturbed compared to pristine graphene. Vacancies significantly increased the work function to >4.7 eV because of a deficiency of electrons in the π -electron system. Experimentally obtained work functions of ‘pristine’ graphene reported in the literature are generally higher than 4.3. eV, which we attribute to be due to the almost unavoidable presence of defects, e.g. at grain boundaries. Substitutional doping of graphitic nitrogen into graphene significantly reduced the work function by donating an extra electron to the π -electron system. Substitutional doping at defects also decreased the work function, but to a lesser extent. Meanwhile, pyridinic nitrogen doping at the edges of vacancies led to a slight increase in work function, because the lone electron pair of pyridinic nitrogen does not interact with the π -electron system. Finally, hydrogen saturation of pyridinic nitrogen atoms reduced the work function, due to a shift towards graphitic-type behavior.

These results hint at key design principles and have important implications for applications where work function engineering is required, such as photocatalysis, electrochemistry, electron field emission, and semiconductor physics (e.g. photovoltaics, organic light emitting diodes). For example, tuning the work function over a wide range could be achieved by a combination of defect engineering, nitrogen doping, and hydrogenation of graphene and other carbon materials. The lowest work functions may be achieved by substitutional nitrogen doping in defect-free graphene, e.g. by chemical vapor deposition.

Acknowledgments

The authors gratefully acknowledge support from the Progress 100 program at Kyushu University and the International Institute for Carbon Neutral Energy Research (WPI-I2CNER), MEXT, Japan. We also acknowledge funding from the Q-Energy Innovator Fellowship fund provided by Kyushu University Platform for Inter- and Transdisciplinary Energy Research. This work was supported by JSPS KAKENHI Grant Numbers JP19H02558 and JP20H00400.


Data availability statement

The data generated and/or analysed during the current study are not publicly available for legal/ethical reasons but are available from the corresponding author on reasonable request.

ORCID iDs

Nikolay Dimov  <https://orcid.org/0000-0003-2950-4272>

Aleksandar Staykov  <https://orcid.org/0000-0003-2572-1317>

Muhammad Irfan Maulana Kusdhany  <https://orcid.org/0000-0003-1076-8462>

Stephen M Lyth  <https://orcid.org/0000-0001-9563-867X>

References

- [1] Zhang S *et al* 2005 Mechanics of defects in carbon nanotubes: atomistic and multiscale simulations *Phys. Rev. B* **71** 1–12
- [2] Banhart F, Kotakoski J and Krasheninnikov A V 2011 Structural defects in graphene *ACS Nano* **5** 26–41
- [3] Li L, Reich S and Robertson J 2005 Defect energies of graphite: density-functional calculations *Phys. Rev. B* **72** 1–10
- [4] Gass M H *et al* 2008 Free-standing graphene at atomic resolution *Nat. Nanotechnol.* **3** 676–81
- [5] El-Barbary A, Telling H, Ewels P, Heggie I and Briddon R 2003 Structure and energetics of the vacancy in graphite *Phys. Rev. B* **68** 1–7
- [6] Lyth S M and Silva S R P 2015 Electron field emission from water-based carbon nanotube inks *ECS J. Solid State Sci. Technol.* **4** P3034–43
- [7] Ziegler D *et al* 2011 Variations in the work function of doped single- and few-layer graphene assessed by Kelvin probe force microscopy and density functional theory *Phys. Rev. B* **83** 1–7
- [8] Filleter T, Emtsev K V, Seyller T and Bennewitz R 2008 Local work function measurements of epitaxial graphene *Appl. Phys. Lett.* **93** 133117
- [9] Yu Y-J *et al* 2009 Tuning the graphene work function by electric field effect. Supplementary Information *Nano Lett.* **9** 3430–4
- [10] Yan L, Punckt C, Aksay I A, Mertin W and Bacher G 2011 Local voltage drop in a single functionalized graphene sheet characterized by Kelvin probe force microscopy *Nano Lett.* **11** 3543–9
- [11] Zhu F *et al* 2014 Heating graphene to incandescence and the measurement of its work function by the thermionic emission method *Nano Res.* **7** 1–8
- [12] Kim J-H *et al* 2013 Work function engineering of single layer graphene by irradiation-induced defects *Appl. Phys. Lett.* **103** 171604
- [13] Sygellou L, Paterakis G, Galiotis C and Tasis D 2016 Work function tuning of reduced graphene oxide thin films *J. Phys. Chem. C* **120** 281–90
- [14] Shi Y *et al* 2010 Work function engineering of graphene electrode via chemical doping *ACS Nano* **4** 2689–94
- [15] Park J *et al* 2011 Work-function engineering of graphene electrodes by self-assembled monolayers for high-performance organic field-effect transistors *J. Phys. Chem. Lett.* **2** 841–5
- [16] Kwon K C, Choi K S, Kim B J, Lee J L and Kim S Y 2012 Work-function decrease of graphene sheet using alkali metal carbonates *J. Phys. Chem. C* **116** 26586–91
- [17] He X *et al* 2015 Tuning the graphene work function by uniaxial strain *Appl. Phys. Lett.* **106** 043106
- [18] Long F *et al* 2016 Characteristic work function variations of graphene line defects *ACS Appl. Mater. Interfaces* **8** 18360–6
- [19] Zeng J J and Lin Y J 2014 Tuning the work function of graphene by nitrogen plasma treatment with different radio-frequency powers *Appl. Phys. Lett.* **104** 2–6
- [20] Akada K, Terasawa T, Imamura G, Obata S and Saiki K 2014 Control of work function of graphene by plasma assisted nitrogen doping *Appl. Phys. Lett.* **104** 131602
- [21] Kresse G and Furthmüller J 1996 Efficient iterative schemes for *ab initio* total-energy calculations using a plane-wave basis set *Phys. Rev. B* **54** 11169–86
- [22] Kresse G and Furthmüller J 1996 Efficiency of *ab-initio* total energy calculations for metals and semiconductors using a plane-wave basis set *Comput. Mater. Sci.* **6** 15–50
- [23] Blöchl P E 1994 Projector augmented-wave method *Phys. Rev. B* **50** 17953–79

- [24] Kresse G and Hafner J 1993 *Ab initio* molecular dynamics for liquid metals *Phys. Rev. B* **47** 558–61
- [25] Momma K and Izumi F 2011 VESTA 3 for three-dimensional visualization of crystal, volumetric and morphology data *J. Appl. Crystallogr.* **44** 1272–6
- [26] Kim J H *et al* 2013 Work function engineering of single layer graphene by irradiation-induced defects *Appl. Phys. Lett.* **103** 171604
- [27] Ding S *et al* 2015 Towards graphane field emitters *RSC Adv.* **5** 105111–8
- [28] Saitoh H *et al* 2002 Work function of amorphous carbon nitride with various functional groups *Japan. J. Appl. Phys.* **41** 6169–73
- [29] Hou Z *et al* 2012 Interplay between nitrogen dopants and native point defects in graphene *Phys. Rev. B* **85** 1–9
- [30] Fujimoto Y and Saito S 2011 Formation, stabilities, and electronic properties of nitrogen defects in graphene *Phys. Rev. B* **84** 1–7
- [31] Tison Y *et al* 2015 Electronic Interaction between nitrogen atoms in doped graphene *ACS Nano* **9** 670–8
- [32] Zitolo A *et al* 2015 Identification of catalytic sites for oxygen reduction in iron- and nitrogen-doped graphene materials *Nat. Mater.* **14** 937–42
- [33] Zitolo A *et al* 2017 Identification of catalytic sites in cobalt-nitrogen-carbon materials for the oxygen reduction reaction *Nat. Commun.* **8** 1–11